Analytical and computational analysis of pressure at the nose of a 2D wedge in high speed flow

Javed S. Shaikh[*1], Krishna Kumar[1a], Khizar A. Pathan[2b] and Sher A. Khan[3]

[1]Department of Applied Sciences and Humanities, MIT School of Engineering, MIT Art,
Design and Technology University, Pune-412201, India
[2]Department of Mechanical Engineering, Trinity College of Engineering and Research, Pune-411048, India
[3]Department of Mechanical Engineering, International Islamic University Malaysia, Kuala Lumpur, Malaysia

Abstract. Supersonic projectiles like rockets, missiles, or aircraft find various applications in the field of defense. The shape of the wings is mainly designed as wedge shape or delta wings for supersonic vehicles. The study of supersonic flows over the wedges and flat plate delta wings around the large scale of incidence angle is considered in the supersonic projectile. In the present paper, the prime attention is to study the pressure at the nose of the plane wedge over the various Mach number and the various angles of incidence. Ghosh piston theory is used to obtain the pressure distribution analytically, and the results are compared with CFD analysis results. The wedge angle and Mach number are the parameters considered for the research work. The range of wedge angle is 50 to 250, and Mach number is 1.5 to 4.0 are considered for the current research work. The analytical results show excellent agreement with the CFD results. The results show that both the parameters wedge angle and Mach number are influential parameters to vary the static pressure. The static pressure increases with an increase in Mach number and wedge angle.

Keywords: CFD analysis; supersonic; wedge angle

1. Introduction

Hypersonic flow is a flow at very high Mach numbers, and the flow behavior is different compared to the supersonic flow. The unsteady hypersonic flow similarity law was first derived by Tisen (1947), which was applied to the extensive scale of Mach numbers. His findings are in good concurrence with the experimental outcomes. Lighthill (1953) evolved the concept of an oscillating airfoil in pitch at a wide range of Mach numbers. Lighthill (1953) found an analytical solution for pitching symmetric airfoils by considering air is perfect gas. Hayes (1947) was studied unsteady flow with high Mach numbers over thin airfoils. The tangent-wedge approximation method and shock expansion theory were used by Zartarian *et al.* (1958) to study unsteady hypersonic flow. Using supersonic flow Mach numbers and the arbitrary angle of attack, Carrier (1949) discovered an exact solution in the 2D flow of an oscillating wedge in the case of the

---

*Corresponding author, Ph.D., E-mail: jss21.aero@gmail.com
[a]Professor, E-mail: krishna.kumar@mituniversity.edu.in
[b]Professor, E-mail: kn.pathan@gmail.com

attached shock wave. Hui (1971) studied and formed the exact solution in an oscillating wedge for 2D flow and derived the solutions for all supersonic Mach numbers and angle of attack with the consideration of attached shock wave for an oscillating flat plate. Lui and Hui (1977) continued Hui's (1971) theory for oscillating flat plate delta wing in pitch with attached shock waves. Ghosh and Mistry (1980) linked Lighthill's (1953) and Mile's (1960) piston theory concept for order of $\emptyset^2$ where $\emptyset$ is the angle between the plane approximates the windward surface and the shock providing the shock wave is attached. Ghosh (1984) has derived similitude with attached leading edge shock at significant incidence in hypersonic flow for delta wings. (Musavir *et al.* 2017, Khan *et al.* 2019) studied the computational and analytical investigation of aerodynamic derivatives in an oscillating wedge. Kalimuthu *et al.* (2019) measured aerodynamic coefficients of without and with spiked blunt body at Mach 6.

Zuhair and Mohammed (2019) have studied trailing edge geometry effect on the aerodynamics of low-speed BWB aerial vehicles. Meng *et al.* (2021) was studied the double-cone missile by the combined spike and multi jet. In the present analysis, the objective is to validate the analytical results of variation of pressure ratio with various Mach numbers and wedge angle by computing different flow parameters for the planar wedge. The CFD analysis is used along with parametric study using ANSYS. The Mach number range was from 1.5 to 4, and the semi-vertex angle of the wedge in the range from 5 to 25 degrees.
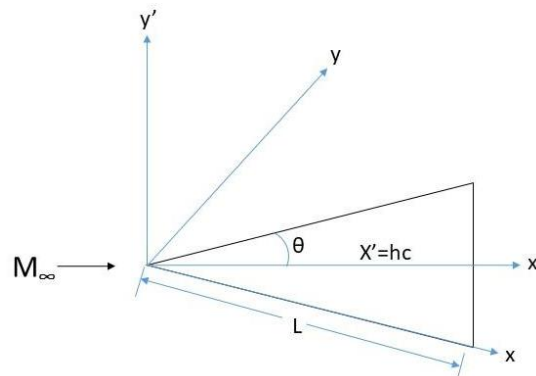

Fig. 1 Geometry of Plane wedge transfer of pivot position from x_0 to x'_0

Consider the flat plate aerofoil be of length L along with the mean wedge angle θ, which oscillates with low amplitude in pitch about the pivot position O_1 and is at a distance x_0 from its apex. At any instant, the angle of attack is α. Then the tiny piston velocity at point x is written in Eq. (1).

$$U_P = U_\infty \sin \alpha + q(x - x_0) \tag{1}$$

The piston Mach number is given by Eq. (2).

$$M_P = M_\infty \sin \alpha + \frac{q(x - x_0)}{a_\infty} \tag{2}$$

Where M_P=Piston Mach number

M_∞=Free stream Mach number

α is the angle of attack

q is pitch rate

a_∞ is free stream velocity

Lighthill (1953) put forward three components in the isentropic expression for the pressure on a piston as in the power series with its velocity to link the piston velocity and pressure on the piston surface. The piston velocity is less than or equal to free stream sound velocity to fulfill the isentropic condition. This is compatible with the theory of small hypersonic disturbance based on the piston theory of Lighthill (1953).

As the velocity component in the *z*-direction is minimum, then the strip of wedge parallel to the centerline can be assumed to be independent along the *z*-direction. This has been explored by Ghosh (1984). It combines the strip theory with the significant incidence similitude of Ghosh's (1984) results in "piston analogy," and surface pressure *P* can be directly connected with corresponding Mach number 'M_p'. In the present case, the flow deflection and piston Mach number 'M_p' are permissible to large. Thus the piston theory of Lighthill or Miles's strong shock piston theory can't be used, but the piston theory of Ghosh's is applied. The surface pressure *P* can directly lead to inertia level at the piston M_p on the wing surface. The expression for pressure distribution is given by the Eq. (3).

$$\frac{P_2}{P_1} = 1 + A(M_P)^2 + AM_P\sqrt{B + (M_P)^2} \tag{3}$$

Where P_2 is pressure on the windward surface

P_1 is freestream pressure

In different span locations, strips are considered to be separate to each other. The wedge angle is the same as that of the wing. In the present situation, both 'M_p' and flow deflection are allowed to be high. The piston theory considered in Eq. (3) also be used in supersonic flow, and the equation can be rewritten as Eq. (4).

$$\frac{P_2}{P_1} = 1 + A\left(\frac{M_P}{\cos\phi}\right)^2 + A\left(\frac{M_P}{\cos\phi}\right)\sqrt{B + \left(\frac{M_P}{\cos\phi}\right)^2} \tag{4}$$

Where ϕ is the angle between wing strip and shock

$$A = \frac{\gamma+1}{4} \quad B = \left(\frac{4}{\gamma+1}\right)^2$$

γ is the specific heat ratio of gas

2. CFD analysis

The Computational Fluid Dynamics (CFD) analysis is done using ANSYS Workbench and Fluent to validate the analytical results. The CFD analysis involved modeling, meshing, and analysis. The Mach numbers considered for the analysis are 1.5, 2.0, 2.5, 3.0, 3.5, and 4.0. The wedge angles considered are 5°, 10°, 15°, 20° and 25°. All possible combinations of parameters for weak solutions are considered for CFD analysis. The air as ideal gas is considered as a fluid for the CFD analysis.
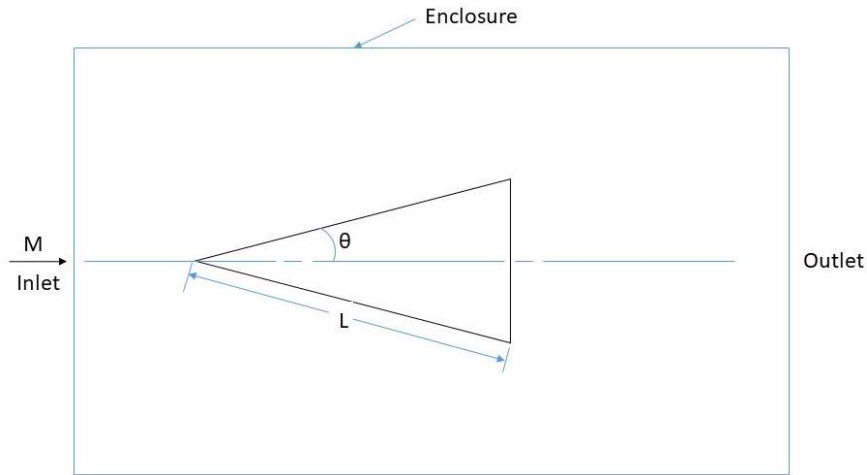
Javed S. Shaikh, Krishna Kumar, Khizar A. Pathan and Sher A. Khan

Fig. 2 2D Geometry of Wedge and enclosure

Table 1 Grid independence test: Number of mesh elements with various element sizes

Mesh Element Size in mm	Mesh Nodes	Mesh Elements
40	944	900
35	1115	1070
30	1253	1189
25	1930	1858
20	2881	2789
15	5113	4989
10	9494	9288
5	37799	37495
4	62295	61963
3	110623	110289
2	236470	236265
1	935685	933681

2.1 Modeling

The modeling is done for all the geometries by varying the wedge angle using the ANSYS design modeler. The geometry for 2D wedge and enclosure is shown in Fig. 2. All the geometries are models by considering the various wedge angle (θ) from 5° to 25°. The length (L)=10 mm is considered for all the models. The enclosure of 3 times length (L) front side, five times length (L) rear side, and five times length (L) at top and bottom sides is created for CFD analysis. The inlet and outlet names are given to the front and rear edges, as shown in Fig. 2.

2.2 Meshing

Before proceeding with the meshing, the grid independence test is an important task to find the optimum mesh element size. The grid independence test has been performed for Mach number 1.5
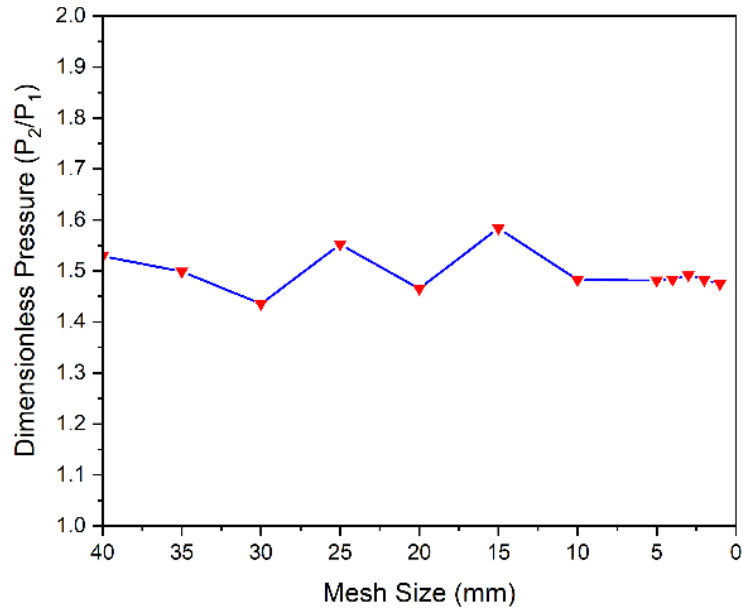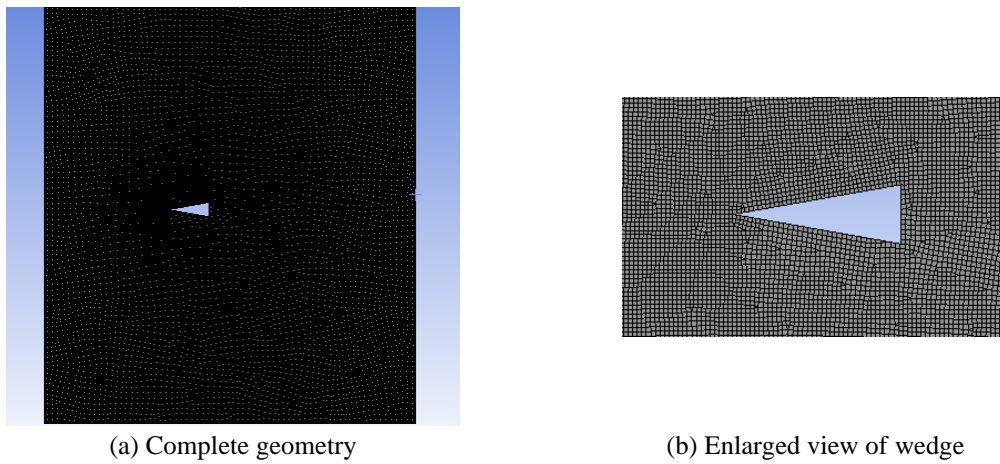
Fig. 3 Grid independence test

(a) Complete geometry   (b) Enlarged view of wedge

Fig. 4 2D meshed geometry for θ=10° and mesh element size 3 mm

and wedges angle 10° by varying mesh size from 1 mm to 40 mm. Table 1 shows the number of elements and nodes for mesh size from 40 mm to 1 mm.

Fig. 3 shows the results of the grid independence test, and from the results, it is clear that at a mesh element size of 10 mm, the result is stable, and the mesh element size of 10 mm can be considered for the CFD analysis. For better accuracy, the mesh element size of 03 mm is adopted for further CFD analysis.

The Hexahedral mesh elements are used in the meshing. Fig. 4 (a) shows the complete meshed model, and Fig. 4(b) shows the enlarged view of the wedge geometry.
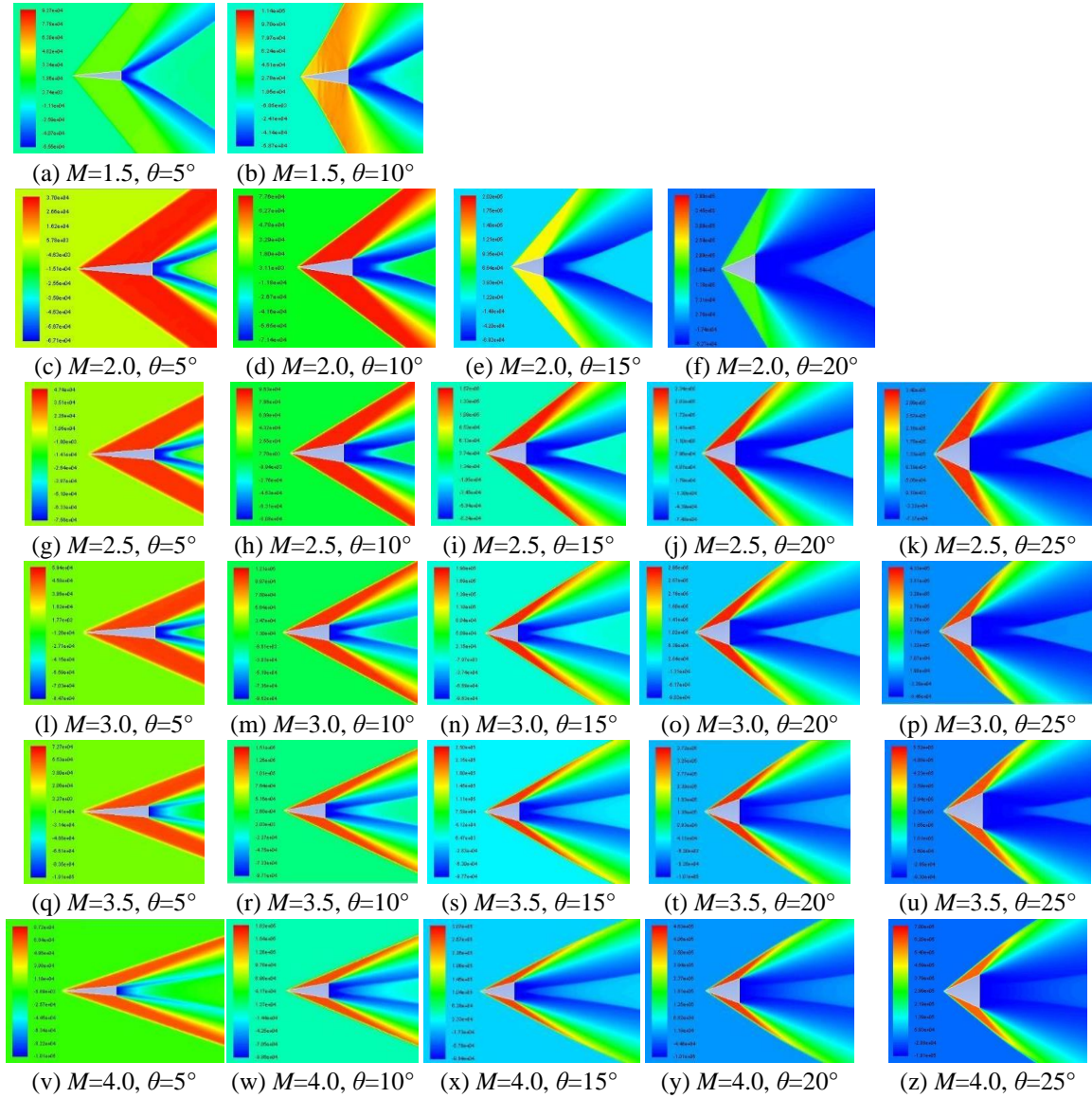
(a) *M*=1.5, *θ*=5°   (b) *M*=1.5, *θ*=10°

(c) *M*=2.0, *θ*=5°   (d) *M*=2.0, *θ*=10°   (e) *M*=2.0, *θ*=15°   (f) *M*=2.0, *θ*=20°

(g) *M*=2.5, *θ*=5°   (h) *M*=2.5, *θ*=10°   (i) *M*=2.5, *θ*=15°   (j) *M*=2.5, *θ*=20°   (k) *M*=2.5, *θ*=25°

(l) *M*=3.0, *θ*=5°   (m) *M*=3.0, *θ*=10°   (n) *M*=3.0, *θ*=15°   (o) *M*=3.0, *θ*=20°   (p) *M*=3.0, *θ*=25°

(q) *M*=3.5, *θ*=5°   (r) *M*=3.5, *θ*=10°   (s) *M*=3.5, *θ*=15°   (t) *M*=3.5, *θ*=20°   (u) *M*=3.5, *θ*=25°

(v) *M*=4.0, *θ*=5°   (w) *M*=4.0, *θ*=10°   (x) *M*=4.0, *θ*=15°   (y) *M*=4.0, *θ*=20°   (z) *M*=4.0, *θ*=25°

Fig. 5 Contours of static pressure for various Mach numbers and wedge angles

2.3 CFD analysis

The CFD analysis is carried out for all the possible combinations of parameters. The *k*-epsilon turbulent model is used for analysis (Khan *et al.* 2019, Pathan *et al.* 2020). Inlet as velocity inlet and outlet as pressure outlet is defined as boundary conditions. Pathan *et al*. (2021) have studied boat tail helmet to reduce drag. The solution is initialized after setting the boundary conditions, and at least 10000 iterations are carried out. The solution seemed to be converged in many cases within 1000 iterations.
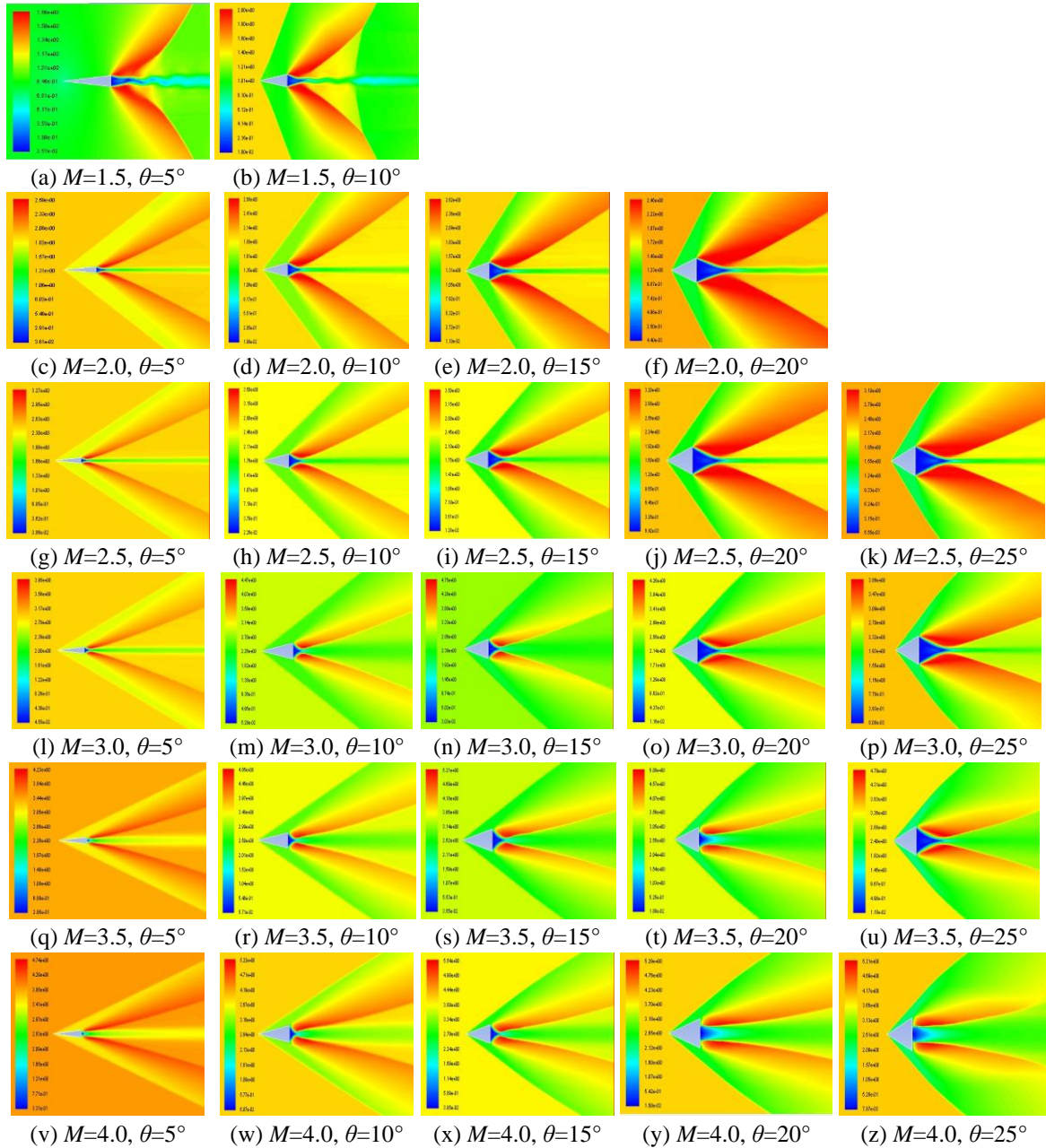
(a) *M*=1.5, *θ*=5°   (b) *M*=1.5, *θ*=10°

(c) *M*=2.0, *θ*=5°   (d) *M*=2.0, *θ*=10°   (e) *M*=2.0, *θ*=15°   (f) *M*=2.0, *θ*=20°

(g) *M*=2.5, *θ*=5°   (h) *M*=2.5, *θ*=10°   (i) *M*=2.5, *θ*=15°   (j) *M*=2.5, *θ*=20°   (k) *M*=2.5, *θ*=25°

(l) *M*=3.0, *θ*=5°   (m) *M*=3.0, *θ*=10°   (n) *M*=3.0, *θ*=15°   (o) *M*=3.0, *θ*=20°   (p) *M*=3.0, *θ*=25°

(q) *M*=3.5, *θ*=5°   (r) *M*=3.5, *θ*=10°   (s) *M*=3.5, *θ*=15°   (t) *M*=3.5, *θ*=20°   (u) *M*=3.5, *θ*=25°

(v) *M*=4.0, *θ*=5°   (w) *M*=4.0, *θ*=10°   (x) *M*=4.0, *θ*=15°   (y) *M*=4.0, *θ*=20°   (z) *M*=4.0, *θ*=25°

Fig. 6 Contours of Mach number at different inlet Mach numbers and wedge angles

3. Results

The CFD and the analytical results are found in excellent agreement. The results obtained by CFD analysis and the analytical results have a maximum of 10% deviation. Fig. 5 shows the static pressure contours for various Mach numbers and angles of incidence. Based on the obtained
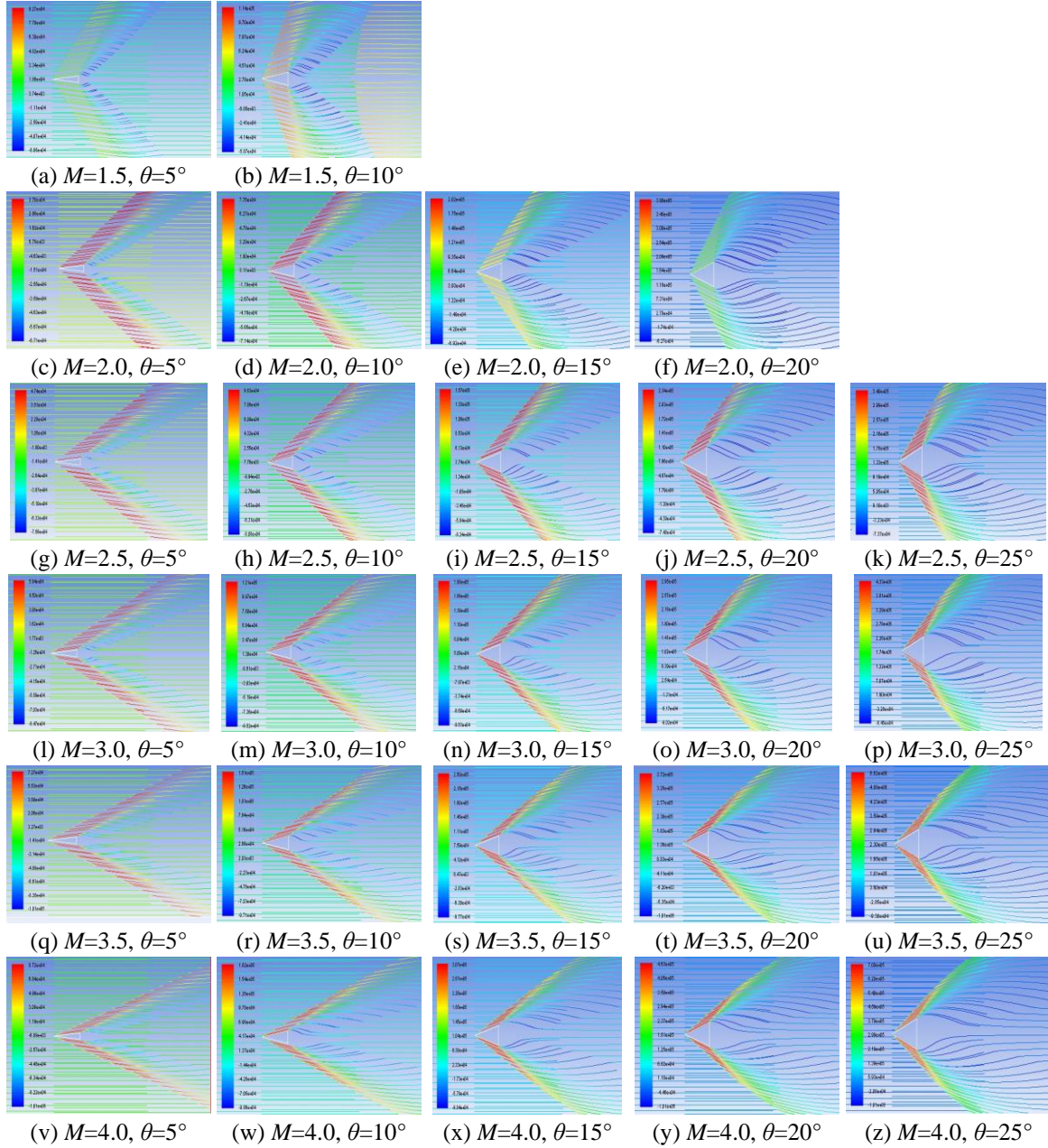
(a) *M*=1.5, *θ*=5° (b) *M*=1.5, *θ*=10°

(c) *M*=2.0, *θ*=5° (d) *M*=2.0, *θ*=10° (e) *M*=2.0, *θ*=15° (f) *M*=2.0, *θ*=20°

(g) *M*=2.5, *θ*=5° (h) *M*=2.5, *θ*=10° (i) *M*=2.5, *θ*=15° (j) *M*=2.5, *θ*=20° (k) *M*=2.5, *θ*=25°

(l) *M*=3.0, *θ*=5° (m) *M*=3.0, *θ*=10° (n) *M*=3.0, *θ*=15° (o) *M*=3.0, *θ*=20° (p) *M*=3.0, *θ*=25°

(q) *M*=3.5, *θ*=5° (r) *M*=3.5, *θ*=10° (s) *M*=3.5, *θ*=15° (t) *M*=3.5, *θ*=20° (u) *M*=3.5, *θ*=25°

(v) *M*=4.0, *θ*=5° (w) *M*=4.0, *θ*=10° (x) *M*=4.0, *θ*=15° (y) *M*=4.0, *θ*=20° (z) *M*=4.0, *θ*=25°

Fig. 7 Pathlines of static pressure for various Mach numbers and wedge angles

results it is seen that with increase in Mach number the Mach cone angle reduces. With increase in wedge angle the base region increases. Fig. 6 shows the Contours of Mach number at different inlet Mach numbers and wedge angles. Fig. 7 shows the pathlines of static pressure for various Mach numbers and angles of incidences. From the results, it is seen that as the Mach number increases with the same wedge angle, the Mach angle reduces. If the shock is extremely weak, the
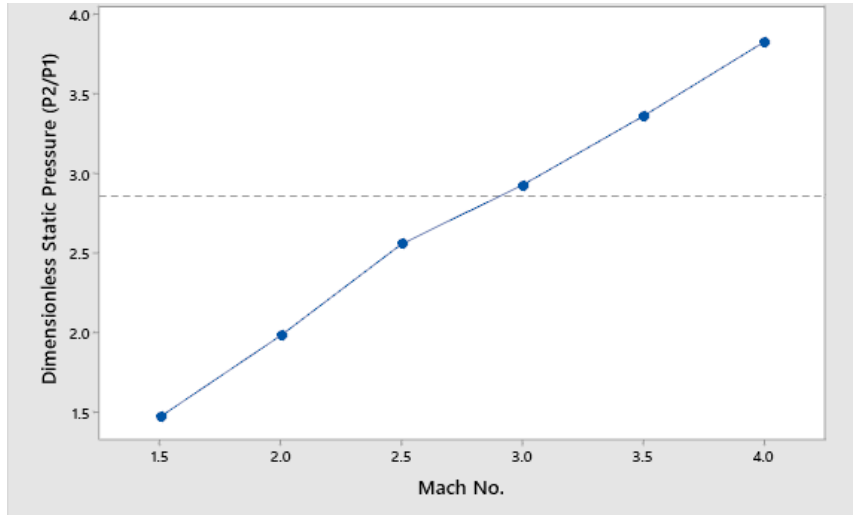
Fig. 8 Effect of Mach number on dimensionless static pressure (P_2/P_1)
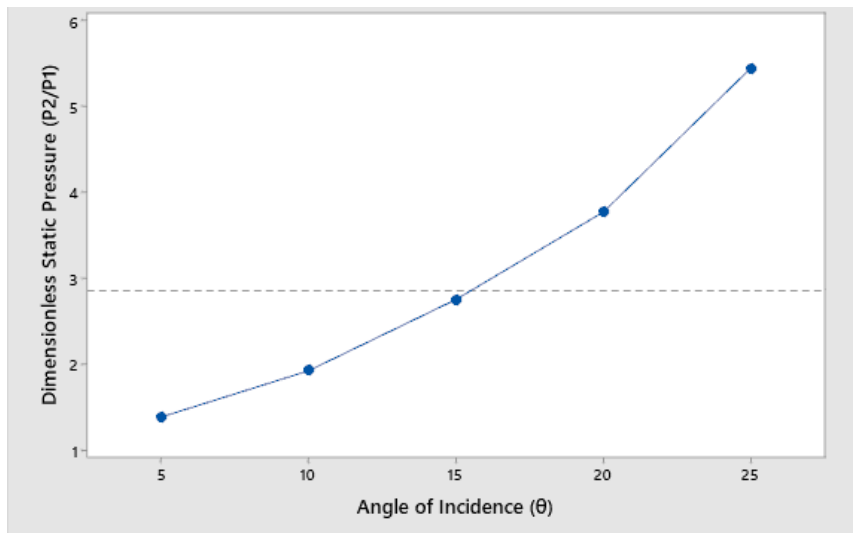

Fig. 9 Effect of wedge angle on dimensionless static pressure (P_2/P_1)

Mach angle (μ) is the same as) shock angle (β). Theoretically, the Mach cone angle (μ) is given by the Eq. (4).

$$\mu = \sin^{-1}\left(\frac{1}{M}\right) \tag{4}$$

It is also seen that as the wedge angle increases, the Mach cone angle increases. The relation between the wedge angle (θ), shock angle (β), and Mach number (M) is given by Eq. (5).

$$\tan\theta = 2\cot\beta\left(\frac{M_1^2 \sin^2\beta - 1}{M_1^2(\gamma + \cos 2\beta) + 2}\right) \tag{5}$$
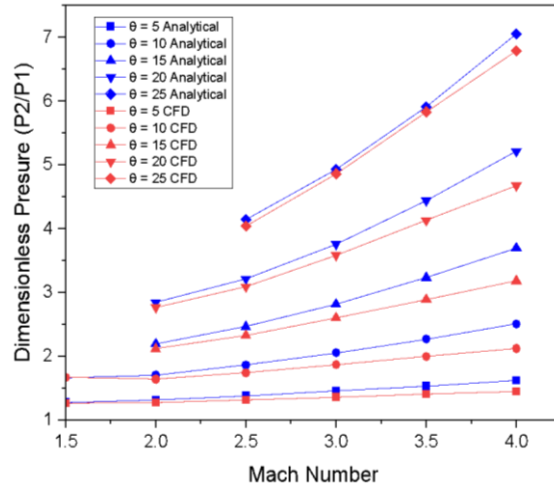
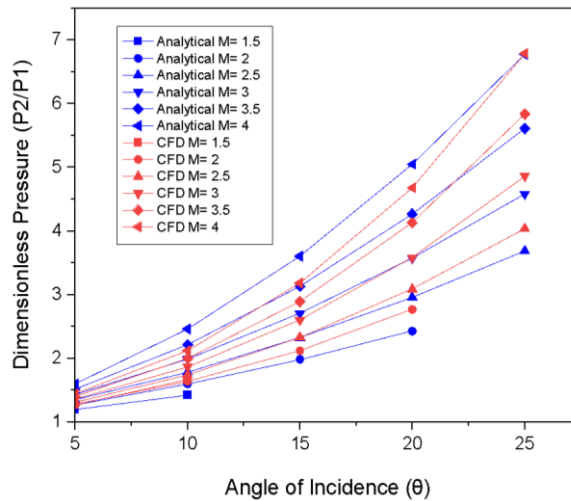Fig. 10 Variation of dimensionless pressure Vs. Mach number

Fig. 11 Variation of dimensionless pressure Vs. wedge angle

The mean values of pressure for all cases are considered and plotted in Fig. 8. Fig. 8 shows the main effect plot for dimensionless static pressure at the nose of the wedge. Based on the obtained results, the static pressure at the nose increases with an increase in Mach number.

Fig. 9 shows the main effect plot for dimensionless static pressure at the nose of the wedge. Based on the obtained results, the static pressure at the nose increases with an increase in the wedge angle.

Fig. 10 shows the variations of dimensionless static pressure at the nose of the Wedge Vs. Mach numbers for various angles of incidence. From the obtained results, it is clear that the CFD and analytical results have an excellent agreement. The absolute static pressure is divided by atmospheric pressure to non-dimensionalized pressure; as Mach number increases, the dimensionless pressure increases. For the lower wedge angle, i.e., $\theta=5°$ and $10°$, the change in

pressure at the nose is marginal with an increase of Mach number from 1.5 to 4.0. As the wedge angle increases, the effectiveness of Mach number increases, and the change of pressure at the nose considerably increases.

Fig. 11 shows the variations of dimensionless static pressure at the nose of the Wedge Vs. wedge angle for various Mach numbers. The static pressure at the nose increases with the wedge angle for all Mach numbers due to the increase in the shock strength. At lower Mach numbers M=1.5 and M=2.0, there is a small growth in pressure for an wedge angle θ=5° and θ=10°. However, as the Mach number increases from M=2.5 to M=4.0, the variation of dimensionless static pressure at the nose of the wedge increases considerably to a large extent with the wedge angle.

4. Conclusions

Ghosh piston theory is used to obtain the pressure distribution analytically, and then the results are compared with CFD analysis results. The CFD and the analytical results shows excellent agreement with the obtained results. It is observed that the variation of dimensionless pressure increases with the Mach number and wedge angle. It is also observed that for the lower wedge angle and lower Mach number, there is a small extent of change in dimensionless static pressure at the nose of the wedge. These results are handy at the design stage of aerospace vehicles as the cost involved in wind tunnel tests is very high. Hence, these results can be used to optimize the design of aerospace vehicles. The present study gives good results with remarkable computational ease.

In future work the researchers may consider various shapes of geometry like ogive with Mach numbers from subsonic, sonic, supersonic and hypersonic.

References

Bashir, M., Khan, S.A., Azam, Q. and Janvekar, A.A. (2017), "Computational and analytical investigation of aerodynamic derivatives of similitude delta wing model at hypersonic speeds", *Int. J. Technol.*, **3**, 366-375. https://doi.org/10.14716/ijtech.v8i3.6319.

Carrier, G.F. (1949), "The oscillating wedge in a supersonic stream", *J. Aeronaut. Sci.*, **16**(3), 150-152. https://doi.org/10.2514/8.11755.

Ghosh, K. (1984), "Hypersonic large deflection similitude for oscillating delta wings", *Aeronaut. J.*, **88**(878), 357-361. https://doi.org/10.1017/S0001924000020868.

Ghosh, K. and Mistry, B.K. (1980), "Large incidence hypersonic similitude and oscillating non-planar wedges", *AIAA J.*, **18**(8), 1004-1006. https://doi.org/10.2514/3.7702.

Hayes, W.D. (1947), "On hypersonic similitude", *Quart. Appl. Math.*, **5**(1), 105-106. https://doi.org/10.1090/qam/20904.

Hui, W.H. (1971), "Supersonic and hypersonic flow with attached shock waves over delta wings", *Proc. Roy. Soc. London. A. Math. Phys. Sci.*, **325**(1561), 251-268. https://doi.org/10.1098/rspa.1971.0168.

Hui, W.H. and Hemdan, H.T. (1976), "Unsteady hypersonic flow over delta wings with detached shock waves", *AIAA J.*, **14**(4), 505-511. https://doi.org/10.2514/3.7120.

Kalimuthu, R., Mehta, R.C. and Rathakrishnan, E. (2019), "Measured aerodynamic coefficients of without and with spiked blunt body at Mach 6", *Adv. Aircraft Spacecraft Sci.*, **6**(3), 225-238. https://doi.org/10.12989/aas.2019.6.3.225.

Khan, S.A., Aabid, A. and Saleel, C.A. (2019), "CFD simulation with analytical and theoretical validation of different flow parameters for the wedge at supersonic mach number", *Int. J. Mech. Mech. Eng.*, **19**(1),

170-177.

Khan, S.A., Fatepurwala, M.A. and Pathan, K.N. (2019), "CFD analysis of human powered submarine to minimize drag", *Int. J. Mech. Prod. Eng. Res. Develop.*, **8**(3), 1057-1066. https://doi.org/10.24247/ijmperdjun2018111.

Lighthill, M.J. (1953), "Oscillating aerofoil at high Mach numbers", *J. Aeronaut. Sci.*, **20**(6), 402-406. https://doi.org/10.2514/8.2657.

Lui, D.D. and Hui, W.H. (1977), "Oscillating delta wings with attached shock waves", *AIAA J.*, **15**(6), 804-812. https://doi.org/10.2514/3.7371.

Miles, J.W. (1960), *Unsteady Flow at Hypersonic Speeds, Hypersonic Flow*, Butterworths Scientific Publications, London, UK.

Pathan, K.A., Dabeer, P.S. and Khan, S.A. (2020), "Enlarge duct length optimization for suddenly expanded flows", *Adv. Aircraft Spacecraft Sci.*, **7**(3), 203-214. https://doi.org/10.12989/aas.2020.7.3.203.

Pathan, K.A., Khan, S.A., Shaikh, A.N., Pathan, A.A. and Khan, S.A. (2021), "An investigation of boat-tail helmet to reduce drag", *Adv. Aircraft Spacecraft Sci.*, **8**(1), 239-250. https://doi.org/10.12989/aas.2021.8.3.239.

Tsien, H. (1946), "Similarity laws of hypersonic flows", *J. Math. Phys.*, **25**(1), 247-251. https://doi.org/10.1002/sapm1946251247.

Zartarian, G., Hsu, P.T. and Ashley, H. (1961), "Dynamic air loads and aeroelastic problems at entry Mach numbers", *J. Aerosp. Sci.*, **28**(3), 209-222. https://doi.org/10.2514/8.8927.

Zuhair, M.A.B. and Mohammed, A. (2019), "Trailing edge geometry effect on the aerodynamics of low-speed BWB aerial vehicles", *Adv. Aircraft Spacecraft Sci.*, **6**(4), 283-296. https://doi.org/10.12989/aas.2019.6.3.225.

EC